Spontaneous deswelling of microgels controlled by counterion clouds

U. Gasser,[1] A. Scotti,[1, 2, 3] and A. Fernandez-Nieves[2, 4, 5]

[1]*Laboratory for Neutron Scattering and Imaging,*
Paul Scherrer Institut, 5232 Villigen, Switzerland
[2]*School of Physics, Georgia Institute of Technology, Atlanta, USA*
[3]*current address: Institute of Physical Chemistry,*
RWTH Aachen University, 52056 Aachen, Germany
[4]*Department of Condensed Matter Physics, University of Barcelona, 08028 Barcelona, Spain*
[5]*ICREA-Institució Catalana de Recerca i Estudis Avançats, 08010 Barcelona, Spain*
(Dated: March 15, 2019)

Concentrated pNIPAM microgel suspensions at a fixed temperature below the deswelling transition of pNIPAM exhibit spontaneous particle deswelling. The microgels deswell before they are in direct contact and, in polydisperse suspensions, this deswelling is most pronounced for the largest microgel particles; as a consequence, the polydispersity of the suspension is reduced. Recently, we presented a model for this spontaneous deswelling that is based on the presence of counterions originating from charged groups on the surface of the pNIPAM microgels [A. Scotti et al., Proc. Natl. Acad. Sci. USA **113**, 5576 (2016)]. Here, we present numerical Poisson-Boltzmann calculations of the electrostatic potential and osmotic pressure inside and outside a pNIPAM microgel that could trigger the observed deswelling at high particle concentrations.

I. INTRODUCTION

Soft colloidal particles are not as well understood as hard, incompressible colloids. In particular, this is the case for high particle concentrations, where the colloids are in close contact and their internal degrees of freedom (deformability, compressibility) become relevant. This is reflected in studies of the interaction and phase behavior of soft colloids in the recent literature. For example, the phase behavior of soft colloidal particles has been studied in Monte Carlo simulations using soft sphere potentials [1–4]; these simulations find a freezing point at higher densities than in hard spheres, consistent with experiments [5, 6]. Furthermore, the Hertzian potential has been used to model the compressibility of soft microgel particles [7–9], and interactions analogous to that of polymer brushes have also been proposed to model the contact interaction between the fuzzy outskirts of swollen microgels [10–12].

Importantly, none of these interactions can account for the remarkable spontaneous deswelling behavior observed in concentrated suspensions of soft microgels that also enables changes in suspension polydispersity. This behavior, not generally observed in other materials, allows crystallization in samples that would otherwise remain in the fluid or glassy state due to polydispersity. It was first observed in mixtures of small and large microgels based on poly(N-isopropylacrylamide) (pNIPAM) [13], where the large particles spontaneously deswelled preventing the formation of the point defects that would otherwise hinder crystallization.

Recently, we have presented a model for this selective deswelling at high concentrations [14] and have shown that the freezing point of polydisperse and bidisperse pNIPAM suspensions is directly linked to particle deswelling [6]. Our findings suggest that the counterions associated to the charged groups at the periphery of pNIPAM microgels and the osmotic pressure they exert at high particle concentrations are the key to the deswelling behavior. Despite pNIPAM is an uncharged polymer, pNIPAM microgels often contain SO_3^- groups originating from ammonium persulfate (APS, $(NH_4)_2S_2O_8$), a common initiator used in the synthesis of the particles; these SO_3^- groups reside at the ends of pNIPAM strands and are located at the periphery of the particles due to mutual electrostatic repulsion and mixing with the solvent [15]. The associated counterions are electrostatically bound to the charged groups forming a cloud that extends both inside and outside the particle. However, a charged sphere cannot bind all of its counterions, and a fraction of them are able to overcome the attraction and wander far from the particle; this happens for entropic reasons and is due to thermal fluctuations. At low microgel volume fractions, ϕ, this small fraction of counterions provides the most important contribution to the osmotic pressure of the suspension. In contrast, at high ϕ, the counterion clouds of neighboring particles overlap, increasing the counterion concentration in the space between the particles. When these overlap-regions take most of the space between particles and percolate through the suspension volume, the previously bound counterions become free to explore the space between the particles, hence contributing to the osmotic pressure of the suspension which, therefore, increases. In our previous work [14], we showed with simple Monte-Carlo simulations that the osmotic pressure due to those counterions outside the particles is indeed higher than that inside the particles for $\phi \gtrsim 0.5$. The counterion concentration inside the particles does not increase with ϕ, as the electrostatic conditions there are mostly unaffected provided the configuration of fixed charges in the particle periphery stays fixed. As a consequence, an osmotic pressure difference, $\Delta\Pi$, builds up between the inside and outside of the microgel particles as the concentration increases.

It is this $\Delta\Pi$ that is responsible for the spontaneous particle deswelling whenever $\Delta\Pi$ is comparable or exceeds the bulk modulus, K, of the particles [14]. At this point, the particles shrink until the elastic stress of the network restores mechanical equilibrium.

In this paper, we adapt numerical Poisson-Boltzmann calculations originally applied to charged colloids [16], to estimate the counterion distribution both inside and outside a charged spherical surface, which we take as a simple model representing the essential electrostatic features of pNIPAM microgels. We find that the resultant osmotic pressure difference between the inside and outside of the particles is consistent with the experimentally observed deswelling of pNIPAM microgels at high particle concentrations.

The paper is structured as follows: We start by reviewing the experiments and discuss both the microgel particles and the observed deswelling at high concentrations. We then present the Poisson-Boltzmann approach and restrict ourselves to the effects of the counterions. We consider the Wigner-Seitz cell for each microgel, and calculate the osmotic pressure at its boundaries, which is related to the counterion concentration in that region, and at the particle center, which also relates to the counterion concentration there; the values of the osmotic pressure obtained in this way agree with those obtained in Monte Carlo simulations. The difference in these pressures qualitatively explains the observed deswelling at high microgel concentrations. We then consider the full free energy of Alexander et. al. [16], and obtain how the inside osmotic pressure is modified due to the electrostatic energy inside the particle; this contribution, however, does not qualitatively change our conclusions. We emphasize that our results for the inside pressure rely on inflating a neutral, impermeable sphere, whose radius is subsequently taken to zero. The last part of the paper is dedicated to explore the effects of salt and how it can eventually eliminate the effects of counterion-induced deswelling. We then conclude, and suggest possible future directions to confirm our results and interpretations.

II. MICROGEL SUSPENSIONS

Microgels are crosslinked polymer networks suspended in a solvent. Depending on the temperature [17, 18], the hydrostatic pressure [19–21], or the pH of the suspension [22, 23], they can exist in swollen or deswollen states, and they can reversibly change from one to the other in response to changes in their environment. pNIPAM microgels are temperature sensitive with a lower critical solution temperature in water of $T_{\mathrm{LCST}} \approx 32\,^\circ\mathrm{C}$. They are swollen for $T < T_{\mathrm{LCST}}$, and deswell for $T > T_{\mathrm{LCST}}$. In the deswollen state, they still contain a significant amount of solvent. The spontaneous deswelling at high concentrations, which is the focus of our work, happens at temperatures below T_{LCST} where particles in dilute conditions are fully swollen.

We have studied pNIPAM microgels containing 2.7 wt% of crosslinker N,N'-methylene-bis(acrylamide) (BIS) with hydrodynamic radii in the range from 110 nm to 190 nm. The details of the particle synthesis are described in the supporting information (SI) of our previous work [14].

Because the crosslinker reacts faster than the NIPAM monomer during synthesis, the microgels have a core-shell structure, with a shell whose polymer density decays from the compact core towards the periphery [18, 24, 25]. Their structure is, therefore, modeled by a spherical core with radius R_{core} and homogenous density that is convoluted with a Gaussian to obtain a shell with decreasing polymer density. This model is well accepted for pNIPAM microgels and correctly describes the measured form factors of our particles [14, 26]. The width of the fuzzy shell is given by 2σ, where σ is the standard deviation of the Gaussian convolution kernel. The polymer density is approximately constant up to a radius $\approx R_{\mathrm{core}} - 2\sigma$, and decays to nearly zero at $R_{\mathrm{SANS}} = R_{\mathrm{core}} + 2\sigma$.

Although pNIPAM is an uncharged polymer, the microgels contain SO_3^- groups that originate from the ammonium persulfate initiator used in the polymerization reaction. During polymerization, the sulfate splits into two SO_4^- groups, which react with carbon double bonds and attach to a carbon chain, C_n, as $SO_3^- - O - C_n\cdot$, where the '$\cdot$' at the end indicates the radical on the distal carbon. The SO_3^- groups remain on the ends of pNIPAM chains and have been found to be located in the particle periphery [15]. The corresponding counterions are ammonium ions (NH_4^+) from the initiator or Na^+ ions from the sodium dodecyl sulfate (SDS) used to control the particle size during synthesis [27]. We note that the SDS is removed with repeated dialysis after the synthesis. Most of the counterions are bound due to strong electrostatic attractions with the fixed SO_3^- groups and form a counterion cloud that can be considered to be part of the microgel particle.

The concentration of colloidal suspensions is often quantified with the volume fraction, ϕ, occupied by the colloidal particles. However for soft and compressible microgels, the particle volume is not straight forward to determine, particularly at high concentrations, and, therefore, we use a generalized volume fraction $\zeta = N_{\mathrm{p}} V_{\mathrm{sw}}/V$, where N_{p} is the number of particles in the suspension, V is the total volume of the suspension, and $V_{\mathrm{sw}} = \frac{4\pi}{3} R_{\mathrm{sw}}^3$ is the fully swollen volume of one microgel, with R_{sw} the radius obtained from dynamic light scattering measurements (see SI of [14] and [28]). In practice, ζ is calculated as

$$\zeta = c\,\frac{\rho_{\mathrm{sol}}}{\rho_{\mathrm{pNIPAM}}}\,\frac{R_{\mathrm{sw}}^3}{R_{\mathrm{coll}}^3}, \qquad (1)$$

where c is the mass fraction of polymer in the suspension, ρ_{sol} and ρ_{pNIPAM} are the mass densities of the solvent and pNIPAM, respectively, and R_{coll} is the particle radius in the fully collapsed state without any solvent in the par-

ticle. The latter is obtained from viscosimetry measurements with dilute suspensions (see SI of [14]). Recall that in these conditions, the microgels are fully swollen and $\zeta = \phi$. At high concentrations, the microgels deform, deswell, and/or interpenetrate and, therefore, ζ can be significantly larger than ϕ and can even exceed 1. In contrast, ϕ is always limited to values ≤ 1 and to $\lesssim 0.74$ in the case of hard spheres.

III. PRIOR RESULTS: DESWELLING AT HIGH ζ

As presented in our previous work, the studied microgels exhibit low interpenetration [14, 26] but deswell at effective volume fractions below random close packing, $\zeta < \phi_{\mathrm{rcp}} \approx 0.64$ [6, 14]. This behavior is revealed with SANS measurements using contrast matching: A small fraction, $(2.9 \pm 0.3)\%$, of large microgels, with swollen radius $R_{\mathrm{l}} = (176 \pm 4)$ nm and that are fully hydrogenated, were suspended with a majority of small particles, with swollen radius $R_{\mathrm{s}} = (117 \pm 7)$ nm, and that are partly deuterated and contrast-matched with H_2O/D_2O solvent. This allows the direct measurement of the form factor of the hydrogenated particles. We followed the spontaneous particle deswelling with this bidisperse suspension to obtain direct measurements of the size of the large particles. The same kind of deswelling is, however, expected in monodisperse suspensions.
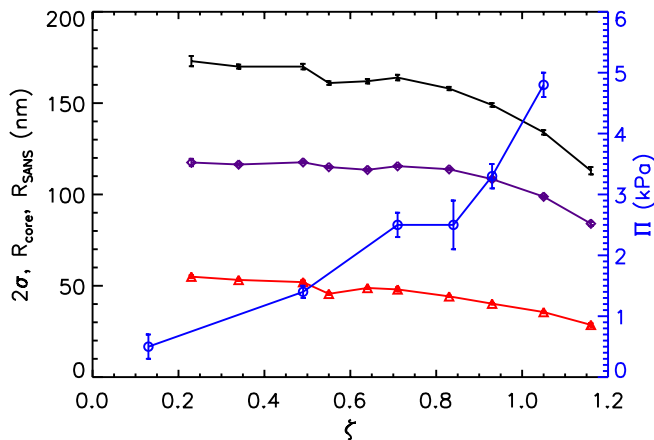

FIG. 1. R_{SANS} (+), R_{core} ($\diamond$), and width of the fuzzy shell, 2σ ($\triangle$), of the large particles in a bidisperse suspension versus ζ as obtained using SANS. The bidisperse suspension contains $(2.9 \pm 0.3)\%$ large particles with swollen radius (176 ± 4) nm and a majority of small particles with radius (117 ± 7) nm. In the range $0.4 < \zeta < 0.7$, the scatter in the data is somewhat larger than the error bars. The latter are obtained from form factor fits carried out independently at each ζ, while the scatter originates from the independent measurements at different ζ. The origin of these two aspects of the data is thus distinct. The right Y-axis shows the osmotic pressure ($\circ$) measured with the same suspension as used for SANS. Data taken from our prior work [14].

Our SANS data show a slight compression of the particles below random close packing, $\zeta < \phi_{\mathrm{rcp}}$; see Fig. 1. The fuzzy shell is found to shrink first, while the core is only compressed for $\zeta \gtrsim 0.8$. This can be understood from the fact that the polymer density decreases towards the particle periphery [18, 25]. Hence, the particle outskirts are expected to be the softest part of the particle and that is why it is compressed first.

We also found that the osmotic pressure is governed by the counterions [14]: At low volume fractions, most of the counterions are bound by the charged groups and form a cloud of counterions on the particle outskirts, extending both inside and outside the particle. The osmotic pressure of the suspension is set by the small fraction of counterions that are weakly bound to the particle and that are able to escape the attraction and explore the whole volume of the suspension. However at high concentrations, the bound counterion clouds of neighboring particles overlap. This causes the counterion concentration to increase in the space between the particles, while the concentration inside the particles shows no marked increase with the concentration of the suspension. Above a critical concentration, ζ^*, we expect the osmotic pressure difference between the outside and inside of the particles to be larger than the bulk modulus of the particles, causing the microgel particle to deswell until mechanical equilibrium is again reestablished. We thus expect the osmotic pressure difference between the outside and inside of the particles to cause the spontaneous deswelling at high concentrations.

From the amounts of NIPAM and ammonium persulfate used in the synthesis of the particles and from the measured particle sizes, we can estimate the number of SO_3^- groups on one particle, as presented in the SI of Ref. [14]. We estimate to have a charge of $-68000e$ on the periphery of one microgel particle, where e is the elementary charge. Osmotic pressure measurements carried out with the suspensions used to study the deswelling of the large particles with SANS show an increase in osmotic pressure, Π, with ζ, as shown by the $\circ$ symbols in Fig. 1. For $\zeta \lesssim 0.8$, $\Pi(\zeta)$ can be approximated to the ideal gas expression: $\Pi = N_{\mathrm{free}} k_{\mathrm{B}} T \zeta / V_{\mathrm{sw}}$, where N_{free} is the number of free counterions per particle. This approximation allows us to estimate N_{free}, which we find corresponds to $8 \cdot 10^3$ free counterions per microgel [14]. As the number of free counterions per particle is $\gg 1$, these free counterions determine the osmotic pressure of the microgel suspension in dilute conditions; note, however, that most counterions are bound to the microgel due to the electrostatic attraction with its fixed charges. For $\zeta \gtrsim 0.8$, the measured $\Pi(\zeta)$ is found to increase faster than linearly. This coincides with the beginning of the strong compression of the large microgels in the binary suspensions. We interpret this as a consequence of a strong overlap of the counterion clouds of neighboring particles, which strongly increases the number of counterions that can effectively unbind in these conditions and contribute to the osmotic pressure of the suspension.

Further, the bulk moduli of our microgels (see SI of Ref. [14]) are expected to decrease with particle size. This is due to the higher reactivity of the crosslinker during synthesis and the fact that the polymerization reaction is left to last longer for larger particles, which means that the crosslinker concentration decays more towards the periphery than for smaller particles, making their outskirts softer. As a consequence of this size-dependent softness, the large particles in the bidisperse suspension deswell before the small ones.

The deswelling due to the overlap of counterion clouds was directly followed with SANS in bidisperse suspensions. However, the same mechanism is at work in monodisperse suspensions, where all particles are expected to deswell in unison when the osmotic pressure due to the counterions exceeds the particle bulk modulus.

IV. POISSON-BOLTZMANN CALCULATIONS

To understand the deswelling in more detail, we use Poisson-Boltzmann calculations to estimate the osmotic pressure given by the counterion cloud at a given ζ.

As the counterions are much more mobile than the microgel particles, we assume the counterions find their equilibrium distribution before the microgels change their configuration in any significant way. Therefore, we consider the charged groups on the microgel surface to be fixed. We model a microgel particle as a sphere with a homogenous surface-charge density that is open for ions to move in and out of the particle through the charged surface. Note that microgels contain a large amount of solvent and, therefore, do indeed have an open structure. The counterions must arrange inside and outside the particle surface such that their charge distribution minimizes their free energy. With the assumption that correlations between counterions are not important, which implies that a mean-field approximation is valid, the equilibrium configuration is given by the Boltzmann factor: $\rho_c(r) = \rho_0 \exp[-\beta e\psi(r)]$, where $\beta = (k_B T)^{-1}$ is the inverse thermal energy and ρ_0 is the counterion density in the region with vanishing electrostatic potential $\psi(r)$. Therefore, the Boltzmann factor $\exp[-\beta e\psi(r)]$ gives the ratio of the probabilities to find a counterion at distance r from the center of the particle and in the region with vanishing $\psi(r)$. The charge density due to the fixed charges on the surface of the particle is $-e\rho_f(r) = -Ze\,\delta(r-R)/(4\pi R^2)$ and gives the second contribution to the total charge density $e\rho(r) = e\{\rho_0 \exp[-\beta e\psi(r)] - \rho_f(r)\}$, where R is the particle radius and Z is the number of charged groups on the particle. The electrostatic potential, $\psi(r)$, is found using the Poisson-Boltzmann equation

$$\Delta\psi(\boldsymbol{r}) = -\frac{e}{\epsilon_r\epsilon_0}\left[\rho_0 e^{-\beta e\psi(\boldsymbol{r})} - \rho_f(\boldsymbol{r})\right]. \qquad (2)$$

Following Alexander et al. [16], we assume every microgel to sit in its Wigner-Seitz cell, which we approximate as a sphere with radius R_c given by the volume fraction of the microgel suspension: $R_c = R\,\phi^{-1/3}$. Due to the spherical symmetry of the model, we use spherical coordinates and thus $\Delta\psi = \frac{1}{r^2}\partial_r\left(r^2\partial_r\psi\right)$. The resulting equation can be solved numerically by iteratively calculating the total charge $eQ(r) = 4\pi\int_0^r dr'\,r'^2\,e\,\rho(r')$ inside the sphere with radius r, the electric field strength $E(r)$, the electrostatic potential $\psi(r)$, and the total density of unit charges $\rho(r) = \rho_c(r) - \rho_f(r)$. The calculation starts at the edge of the cell at $r = R_c$, where $Q(R_c) = 0$, $E(R_c) = 0$, and $\rho(R_c) = \rho_c(R_c) = \rho_0$, with $\rho_c(r)$ the counterion density. The calculation proceeds towards $r = 0$ using the equations

$$\begin{aligned} Q(r) &= Q(r+dr) - 4\pi\,r^2\,dr\,\rho(r+dr) \qquad (3)\\ E(r) &= \frac{eQ(r)}{4\pi\,\epsilon_r\epsilon_0 r^2}\\ \psi(r) &= E(r)dr + \psi(r+dr)\\ \rho(r) &= \rho_c(r) - \rho_f(r) = \rho_0\exp[-\beta e\psi(r)] - \rho_f(r). \end{aligned}$$

Using Eqs. 3, we obtain the number of charges inside the sphere with radius r from the number of charges in the larger sphere with radius $r + dr$. The quantities $E(r)$, $\psi(r)$, and $\rho(r)$ are then calculated at the reduced radius r. Note that this procedure does indeed give a solution of the Poisson-Boltzmann equation. For the calculation of $E(r)$, we use Gauss' law: For a spherically symmetric arrangement of charges, the E-field at distance r from the center is given by the total charge in the sphere with radius r and equals the field of the total charge concentrated in the center. This guarantees that the Poisson equation for the spherically symmetric problem $-\Delta\psi(r) = \partial_r E(r) = e\rho(r)/(\epsilon_0\epsilon_r)$ is fulfilled. Further, $\rho_c(r)$ is calculated using the Boltzmann factor. Also note that the fixed charges are located at $r = R$ and, therefore, have to be taken into account when r is reduced from $r > R$ to $r < R$. At this point, $Q(r)$ is reduced by the number of fixed charges, Z.

We also use the boundary condition $\frac{d\psi}{dr}(R_c) = 0$, as the total charge inside the Wigner-Seitz cell equals zero and, as a consequence, the E-field at $r = R_c$ vanishes. We can also require that $\psi(R_c) = 0$, which we indeed do, as the potential can be varied with an arbitrary constant.

The only free parameter in the iterative calculation is the counterion density at the edge of the cell, $\rho_c(R_c) = \rho_0$. The calculation is started with an estimation for ρ_0. Whether that ρ_0 gives the solution, is checked at the end of each round by calculating the total mobile charges $4\pi\int_0^{R_c} dr\,r^2\,\rho_0\exp[-\beta e\psi(r)]$, which must equal the number of fixed charges, Z, due to charge neutrality. If this condition is not fulfilled within the desired accuracy, ρ_0 is corrected and the next round is started. By solving the Poisson-Boltzmann problem, we thus fix ρ_0, the potential $\psi(r)$, and the counterion density $\rho_c(r)$.

The calculated electrostatic potential for three volume fractions of the suspension is shown in Fig. 2a. The potential $\psi(0)$ in the center of the particle increases relative to $\psi(R_c) = 0$ at the boundary of the cell, as ϕ increases
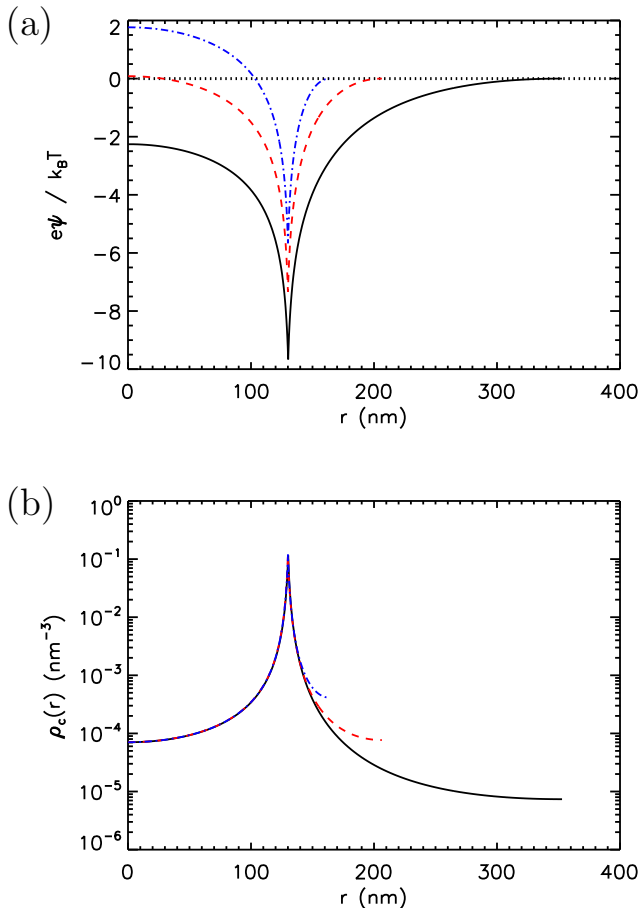
FIG. 2. (a) Electrostatic potential for a particle with radius 130 nm and $Z = 70000$ mobile charges for the volume fractions $\phi = 0.05$ (—), 0.25 ($- - -$), and 0.50 ($- \cdot -$). The curves end at $r = R_c$, where $\psi(R_c) = 0$. (b) The corresponding counterion densities. For $r \lesssim 140$ nm, all three densities virtually agree.

from 0.05 to 0.5. While $\psi(0)$ is lower than $\psi(R_c)$ for $\phi = 0.05$, it is higher for $\phi = 0.5$. This behavior is reflected by the counterion density shown in Fig. 2b. In dilute conditions (e.g. $\phi = 0.05$), the counterion density inside the particle is larger than that at the edge of the cell. However, the situation is reversed at high concentrations (e.g. $\phi = 0.5$), and this reversal is a consequence of the proximity of neighboring particles causing the counterion clouds to overlap in the space between particles. We note that the counterion density has its maximum at $r = R$, where the electrostatic energy of a counterion, $e\psi(r)$, is minimal. Also, the counterion density inside the particle is virtually independent of ϕ. This is expected, as the environment of the counterions inside the particle remains almost unaffected by a change in the available space outside the particle with a change in ϕ. Also note that, in contrast to the counterion density, $\psi(r)$ shows a large change for $r < R$ as ϕ is varied from 0.05 to 0.5. This is a consequence of our boundary condition

$\psi(R_c) = 0$.

The Poisson-Boltzmann calculation treats the counterion cloud in a mean-field approximation that is expected to break down when correlations between counterions become important. This would occur first at the minimum of $\psi(r)$, where the concentration of counterions is highest (see Figs. 2a and b). We use our Monte-Carlo simulations of the counterion cloud presented in the SI of Ref. [14] to estimate this effect. The simulations assume $Z = 7 \cdot 10^4$ mobile counterions with charge e that arrange around a smooth spherical surface charge $-Ze$ at $R = 130$ nm. The counterions are confined to a spherical Wigner-Seitz cell and are treated as hard spheres with radius $0.01\,l_B$, where $l_B \approx 0.7$ nm is the Bjerrum length in water at $T \approx 20°$C. The counterions are virtually point like, as their radius is much smaller than l_B. We take the counterion positions in a thin spherical shell of thickness given by the Bjerrum length around the particle radius, $r = R$, and calculate the pair distribution function $g(s)$, where s is the distance from an ion within the thin spherical shell to a neighbouring ion also located in the shell. The results for $\phi = 0.05$, 0.25, and 0.5 are shown in Fig. 3. The Coulomb repulsion of the counterions is apparent from the correlation hole, which has an approximate width of ≈ 2 nm. The structure of the counterion cloud appears to be gas like, as $g(s)$ approaches a constant value without showing the peaks that would indicate the presence of shells of nearest or higher order neighbor correlations and that would reflect the existence of local-range order. The correlation hole has the size expected from the nearest-neighbor distance following from the peak value of $\rho_c(r)$ shown in Fig. 2b: $d_{nn} = 2[3/(4\pi\rho_{c,peak})]^{1/3} \approx 2.7$ nm. These results confirm the validity of the Poisson-Boltzmann approach.
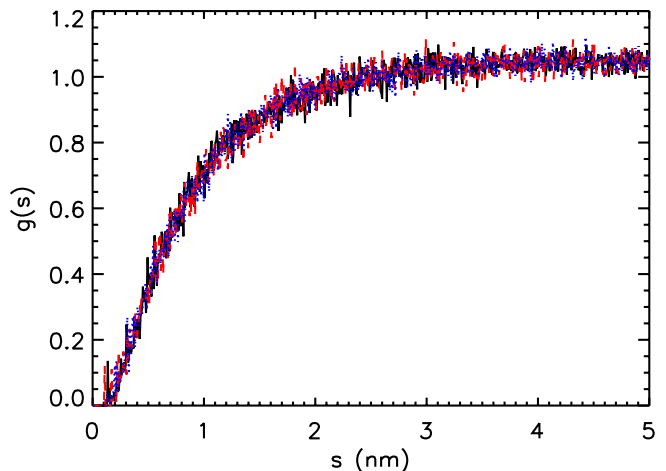

FIG. 3. Pair distribution functions of counterions in a spherical shell with thickness 0.7 nm at the potential minimum at the particle radius $R = 130$ nm. The volume fractions are $\phi = 0.05$ (—), $\phi = 0.25$ (— —), and $\phi = 0.50$ (· · ·).

V. OSMOTIC PRESSURE

The osmotic pressure due to the counterions is obtained as the partial derivative of the Helmholtz free energy with respect to the volume of the Wigner-Seitz cell with T and Z fixed:

$$\Pi = -\left(\frac{\partial F}{\partial V}\right)_{T,Z}. \tag{4}$$

We first use a simplified free energy that includes the mobile counterions but neglects the fixed charge on the surface of the microgel: $F = -k_\mathrm{B}T \ln \mathcal{Z}$ with $\mathcal{Z}$ the configurational integral of the counterions inside the Wigner-Seitz cell. The kinetic energy of the ions is omitted, as it contributes a mean energy $\frac{3}{2}Zk_\mathrm{B}T$, which is constant as long as T and Z are fixed. Since the Poisson-Boltzmann equation follows from a mean-field approach, correlations between counterions are assumed negligible, and each counterion is thought to experience the same environment, with the presence of other ions entering only via $\psi(r)$. Therefore, the configurational integral can be written as $\mathcal{Z} = z^Z$, where

$$z = 4\pi \int_0^{R_\mathrm{c}} dr\, r^2 e^{-\beta e \psi(r)}. \tag{5}$$

is the configurational integral of a single counterion. Thus, $F = -k_\mathrm{B}T \log z^Z$. Note this procedure is analogous to that followed in developing the van der Waals model of a fluid, which is also a mean-field theory assuming equivalent environments for all molecules in the fluid and that also neglects correlations between the molecules; the many-particle configurational integral of the van der Waals model is, therefore, also written as the product of the configurational integrals of single molecules.

With this, we obtain the osmotic pressure

$$\begin{aligned}
\Pi &= -\frac{1}{4\pi R_\mathrm{c}^2}\left(\frac{\partial F}{\partial R_\mathrm{c}}\right)_{T,Z} \\
&= \frac{1}{4\pi R_\mathrm{c}^2}\left(\frac{\partial}{\partial R_\mathrm{c}} k_\mathrm{B}T \log z^Z\right)_{T,Z} \\
&= k_\mathrm{B}T \frac{Z}{z} = k_\mathrm{B}T\, \rho_0.
\end{aligned} \tag{6}$$

where we have used the first fundamental theorem of integral calculus. The osmotic pressure of the suspension then only depends on temperature and the counterion density at the edge of the Wigner-Seitz cell, where $E(R_\mathrm{c}) = 0$. At this location, the counterions are thus 'free', hence determining Π. We emphasize that the mean-field approach gives the same result as a more fundamental treatment of the problem taking all the electrostatic interactions of the mobile ions and the fixed charged surface into account without relying on the mean-field approximation of the Poisson-Boltzmann theory [29, 30].

To estimate the osmotic pressure due to the counterions inside the particle, Π_i, we again only consider the free energy due to the counterions and fix the cell radius R_c but think of a small, spherical volume with radius ϵ in the center of the particle that is enclosed by a semipermeable membrane, which is open for the solvent but does not let the ions through – this is a usual setting to calculate an osmotic pressure. Therefore, no mobile ions are allowed in this small volume. This implies that the integration range for the configurational integral starts at the hard-sphere radius ϵ:

$$z(\epsilon) = 4\pi \int_\epsilon^{R_\mathrm{c}} e^{-\beta e \psi(r)} r^2\, dr.$$

The osmotic pressure in the particle center is then obtained from the derivative of the free energy with respect to this excluded volume, taking the limit $\epsilon \to 0$ subsequently:

$$\begin{aligned}
\Pi_\mathrm{i} &= \frac{1}{4\pi\,\epsilon^2}\left(\frac{\partial F}{\partial \epsilon}\right)_{T,Z} \\
&= -k_\mathrm{B}T \frac{Z}{z(\epsilon)}\left(\frac{\partial z(\epsilon)}{\partial \epsilon}\right)_{T,Z} \\
&= k_\mathrm{B}T \frac{Z}{z(\epsilon)} e^{-\beta e \psi(\epsilon)} \\
&\overset{\epsilon \to 0}{\to} k_\mathrm{B}T \frac{Z}{z} e^{-\beta e \psi(0)} = k_\mathrm{B}T\, \rho(0).
\end{aligned} \tag{7}$$

Similarly to the osmotic pressure outside the particle, the osmotic pressure inside the particle is given by the density of 'free' counterions at $r = 0$, where $E(0) = 0$ due to the spherical symmetry.

The osmotic pressure outside $(+)$ and our estimate for the pressure inside $(*)$ a microgel particle are shown in Fig. 4, where we also show the measured osmotic pressure $(\circ)$ for comparison. The mean-field approximation used to calculate this Π_i also gives the same result as the more fundamental approach presented in the Appendix.

To confirm our results, we also use Monte-Carlo simulations and obtain the osmotic pressure through the well known relation [31]:

$$\Pi = k_\mathrm{B}T\rho + \frac{1}{3V}\left\langle \sum_i \boldsymbol{r}_i \cdot \boldsymbol{f}_i \right\rangle, \tag{8}$$

where $\boldsymbol{r}_i$ is the position of counterion i, and $\boldsymbol{f}_i$ is the total force acting on this ion, which includes the force due to the other counterions and the force due to the fixed charge:

$$\boldsymbol{f}_i = \sum_{\substack{k=0 \\ k \neq i}}^{Z} \frac{k_\mathrm{B}T\, l_\mathrm{B}}{|\boldsymbol{r}_i - \boldsymbol{r}_k|^2} \frac{\boldsymbol{r}_i - \boldsymbol{r}_k}{|\boldsymbol{r}_i - \boldsymbol{r}_k|} + \begin{cases} 0 & r_i \leq R \\ \frac{-k_\mathrm{B}T\, l_\mathrm{B}Z}{r_i^2}\frac{\boldsymbol{r}_i}{r_i} & r_i > R \end{cases}.$$

We estimate Π_i by averaging over all counterions within $0 \leq r < 0.5R$ in Eq. 8. This is done for 10 time-steps of the simulation after it has reached the equilibrium state. One simulation was performed for each volume fraction ϕ. The values of Π_i are comparable to those obtained

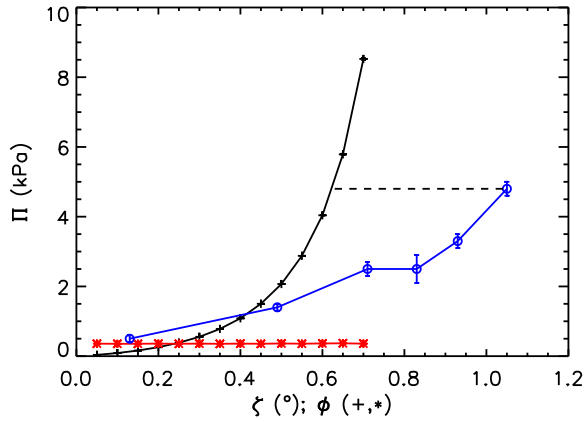FIG. 4. (○) Osmotic pressure obtained from osmometry measurements versus effective volume fraction, ζ, and (+) osmotic pressure obtained from numerical Poisson-Boltzmann calculations as a function of volume fraction, ϕ. The calculated pressure inside the microgels is shown by (∗) symbols. The dashed horizontal line at the osmotic pressure $\Pi = 4.8$ kPa maps the measurement at $\zeta = 1.05$ and the calculation at $\phi = 0.63$.

TABLE I. Inside osmotic pressures obtained for $R = 130$ nm and $Z = 70000$. Calculations are done using Eq. 7. Eq. 8 is used to obtain pressures from Monte-Carlo simulations. For each simulation, pressures calculated from 10 times-steps taken after the simulation has reached the equilibrium state are averaged and the errors reflect the variation of these 10 pressures.

ϕ	Π_i (Pa)	
	calculation	simulation
0.05	287 ± 2	$(21 \pm 2) \cdot 10$
0.25	292 ± 6	$(22 \pm 3) \cdot 10$
0.5	285 ± 1	$(21 \pm 3) \cdot 10$

using Eq. 7, as shown in Table I. This indicates that our calculation using Eq. 7 is reasonable.

We emphasize that our simplified free energy only considers the counterions and neglects the electrostatic contribution due to the fixed surface-charge. We will, however, see in Section VII that including this contribution does not qualitatively change the results. In addition, it is worth emphasizing that our result for the inside osmotic pressure relies on deflating a neutral, impermeable sphere in a sea of charged counterions. While this approach is certainly valid for obtaining the pressure of neutral gases and liquids, it may require further assessment for charged systems. The agreement with the Monte Carlo simulation results, however, suggests that it may nevertheless be a reasonable approximation. However, additional theoretical work, maybe based on the approach presented in [32], is needed to more rigorously

calculate Π_i.

VI. COMPARISON WITH EXPERIMENTAL RESULTS

In Fig. 4, we plot the calculated osmotic pressure, Eqs. 6 and 7, and the results from osmometry. For small ζ, calculation (+) and measurement (○) are comparable. With increasing ζ, the measured osmotic pressure does not increase as fast as the calculated osmotic pressure. This reflects particle deswelling and the additional volume the free counterions have available due to the reduced particle size. We use the data shown in Fig. 4 to estimate the actual volume fraction, ϕ, for a given ζ. We do this by mapping the calculated osmotic pressure in the outside of the particles onto the experimental measurements. For instance, we obtain that the suspension at $\zeta = 1.05$ with osmotic pressure $\Pi = 4.8 \pm 0.2$ kPa corresponds to an actual volume fraction $\phi \approx 0.62$ (see dashed line in Fig. 4). Remarkably, the random close packing limit, $\phi_{\rm rcp}$, is not reached at $\zeta = 1.05$, the highest concentration we used in our osmometry measurements. This confirms that particle deswelling happens in the absence of direct interactions between the microgels.

From the $\phi(\zeta)$ estimates, we calculate the actual ζ-dependent particle radius as $R_{\rm sc}(\zeta) = [\phi(\zeta)/\zeta]^{1/3} R_{\rm s}$, where the subindex sc indicates the corrected, swollen radius. To compare this calculated deswollen radius with measurements, we plot the ratio $R/R_{\rm coll}$ in Fig. 5, where R is either the calculated radius $R_{\rm sc}(\zeta)$ or a measured radius $R(\zeta)$ obtained using SANS, and $R_{\rm coll}$ is the radius in the collapsed state. We find that the calculated ratio (□) is close to the measured ratios for the deswelling of large particles in a suspension with a $(97.1 \pm 0.3)\%$ majority of small particles (△) and for the deswelling of small particles in a suspension with $(84 \pm 3)\%$ of large particles (◇). Therefore, our model for the pressure-induced deswelling at high concentrations appears to qualitatively capture the deswelling mechanism. This agreement is obtained with the rather simple model presented above for the solution of the Poisson-Boltzmann equation and without taking any details of the microgel structure into account. The only particle property enabling deswelling is the particle bulk modulus; if too large, deswelling might be hindered.

To more realistically model pNIPAM microgels, we consider that the fixed charges are smeared out around a spherical shell with radius R. This accounts for the SO_3^- groups being fixed to the ends of pNIPAM chains, which are crosslinked to other chains. The charged ends of the chains are expected to be located near the periphery of the particle [15], and we use a Gaussian distribution centered at R to account for this. This broader distribution of the fixed charges reduces the depth of the minimum in $\psi(r)$ compared to the simpler model presented above, as shown in Fig. 6a. As a consequence, the counterions are somewhat more spread out, and the osmotic pressure
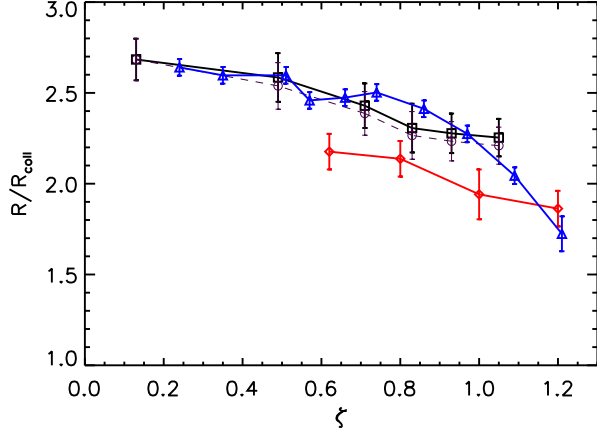
(a)

(b)

FIG. 5. Radius ratio R/R_{coll} versus effective volume fraction ζ for the ($\square$) calculated deswelling of microgels with swollen radius $R_{\mathrm{sw}} = 117$ nm and collapsed radius $R_{\mathrm{coll}} = 43.6$ nm, and the ($\diamond$) deswelling measured by SANS for microgels with swollen radius $R_{\mathrm{SANS}} = (137 \pm 4)$ nm and collapsed radius $R_{\mathrm{coll}} = (51.0 \pm 0.6)$ nm, as well as with ($\triangle$) $R_{\mathrm{SANS}} = (176 \pm 4)$ nm and $R_{\mathrm{coll}} = (65.5 \pm 0.4)$ nm. Note $R_{sw}/R_{coll} = R_{SANS}/R_{coll} = 2.68$. The calculation for the case of a spread-out cloud of fixed charges is shown by the ($\circ$) symbols with dashed line.
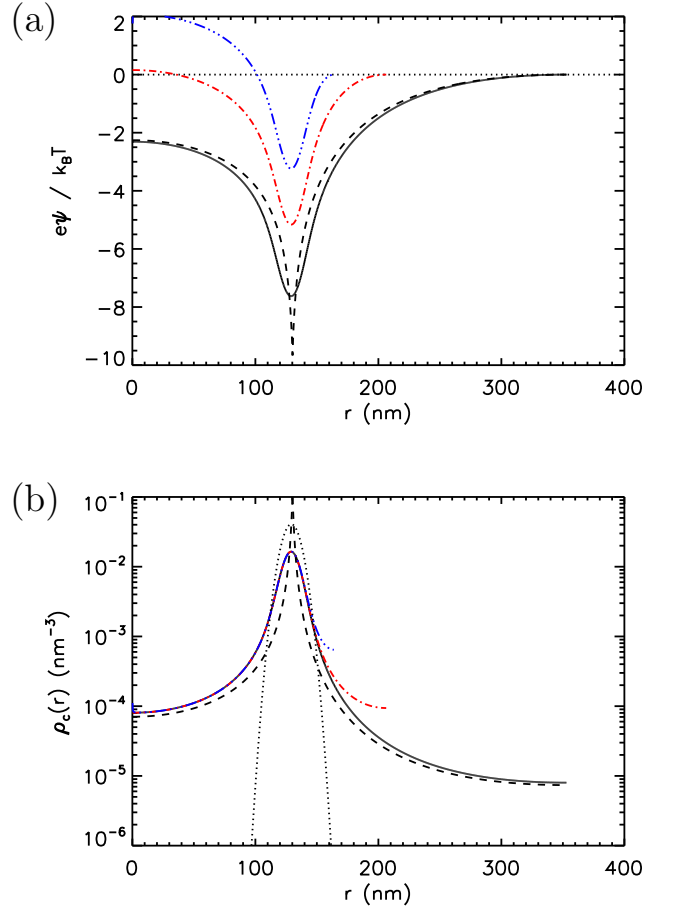
FIG. 6. (a) Electrostatic potential for a particle with radius 130 nm and a Gaussian distribution of the fixed charges with mean deviation 14.3 nm for the volume fractions $\phi = 0.05$ (—), 0.25 (—·—), and 0.50 (—··—). The potential corresponding to when the fixed charges are concentrated at $r = R_{\mathrm{SANS}}$ and $\phi = 0.05$ is shown by the dashed curve (— — —). $\psi(r) = 0$ is highlighted with a horizontal dotted line. (b) Corresponding counterion densities. The density distribution of the fixed charges is shown by the dotted curve (···).

is slightly increased, as can be seen from the counterion densities shown in Fig. 6b. Due to the higher osmotic pressure, the deswelling at high concentrations is slightly stronger with a broader distribution of the fixed charges at the microgel periphery. This is shown by the ($\circ$) symbols in Fig. 5, which show R/R_{coll} for spread-out fixed charges and appear below the symbols representing the case with all fixed charges on a spherical surface ($\square$). However, this effect is small, indicating that the approximation with all fixed charges located on a thin spherical shell is reasonable.

As shown by the ($+$) and ($*$) symbols in Fig. 4, the osmotic pressure of the microgel suspension is expected to exceed the osmotic pressure inside the microgel particles for $\phi \gtrsim 0.24$. This osmotic pressure difference suggests that the softest part of a microgel particle, the fuzzy corona, might deswell before a strong overlap of the counterion clouds is reached and the particle shows pronounced deswelling. This is observed in Fig. 1, where the fuzzy shell of the microgels seems to decrease from $2\sigma \approx 55$ nm at $\zeta = 0.23$ to ≈ 49 nm at $\zeta = 0.64$, while the core of the particle essentially retains its size.

Since the swelling of a microgel is given by the balance of the osmotic pressures inside and outside the particle [33], we can estimate the bulk modulus from the calculated and measured osmotic pressures. As the first signs of deswelling are found at $\zeta \approx 0.23$ in our SANS measurements and as the calculated osmotic pressure outside the particles starts to exceed the osmotic pressure inside the particles at about the same ζ (Fig. 4), we estimate the

bulk modulus of the fully swollen microgel at $\zeta \lesssim 0.23$ to be given by our calculated osmotic pressure at $\zeta = 0.23$: $K_{\mathrm{sw}} \approx 300$ Pa. This value is in good agreement with the Young's modulus of swollen pNIPAM particles determined using Atomic Force Microscopy [34]. The bulk modulus of the core is obtained from the osmotic pressure at $\zeta \approx 0.8$, where the core starts to be compressed. We find $K_{\mathrm{core}} = (2.5 \pm 0.2)$ kPa. Comparing with the literature, bulk moduli on the same order of magnitude have been reported for pNIPAM-based microgels at high concentrations or in the deswollen state [34, 35].

VII. OSMOTIC PRESSURE INCLUDING COUNTERIONS AND FIXED CHARGE

Here, we use the free energy $F = U - TS$ [16], where U is the total electrostatic energy

$$U = \frac{4\pi e}{2} \int_0^{R_c} dr\, r^2 \left[\rho_c(r) - \frac{Z}{4\pi R^2}\delta(r-R) \right] \psi(r)$$

and $S = -Z k_B \int d^3r\, p(r) \log p(r)$ is the entropy due to the mobile counterions, with $p(r) = \frac{1}{z}e^{-\beta e\psi(r)}$ the normalized probability density to find a counterion at distance r from the center and z the configurational integral of a single counterion given in Eq. 5. Writing the entropy as

$$S = -Z k_B\, 4\pi \int_0^{R_c} dr\, r^2\, p(r)\left[-\log z - \beta e\psi(r) \right]$$

$$= Z k_B \log z + \frac{4\pi}{T}\int_0^{R_c} dr\, r^2 \psi(r) e\rho_0 e^{-\beta e\psi(r)},$$

the free energy becomes:

$$F = -\frac{Ze}{2}\psi(R) - Z k_B T \ln z$$

$$-2\pi \int_0^{R_c} dr\, r^2\, \psi(r)\, e\rho_0 e^{-\beta e\psi},$$

where we have used the counterion density $\rho_c(r) = \frac{Z}{z}e^{-\beta e\psi(r)} = \rho_0 e^{-\beta e\psi(r)}$. We take ρ_0 to be constant, as in Ref. [16], and equal to the value obtained by self-consistently solving the Poisson-Boltzmann equation, see section IV.

To obtain the outside osmotic pressure due to the counterions we vary the volume of the spherical Wigner-Seitz cell by considering small changes of the cell radius R_c.

$$\Pi = -\frac{1}{4\pi R_c^2}\left(\frac{\partial F}{\partial R_c} \right)_{T,Z}$$

$$= \frac{1}{4\pi R_c^2}\left(\frac{\partial}{\partial R_c} Z k_B T \log z \right)_{T,Z}$$

$$+ 2\pi R_c^2 \psi(R_c)e\rho_0 e^{-\beta a\psi(R_c)}$$

$$= k_B T \frac{Z}{z} = k_B T\, \rho_0,$$

where we have used that $\psi(R_c) = 0$. We obtain the same result as with the simplified free energy used in section V, which did not include the electrostatic energy.

To estimate the osmotic pressure inside the charged spherical surface, we again consider a small, spherical volume with radius ϵ located at the center that is not allowed to contain counterions, as done in section V. Due to the hard repulsion of counterions at $r = \epsilon$, there are no charges for $r < \epsilon$. The free energy now becomes:

$$F = -\frac{Ze}{2}\psi(R) - Z k_B T \ln z(\epsilon)$$

$$-2\pi \int_\epsilon^{R_c} dr\, r^2\, \psi(r)\, e\rho_0 e^{-\beta e\psi(r)}$$

with

$$z(\epsilon) = 4\pi \int_\epsilon^{R_c} e^{-\beta e\psi(r)} r^2\, dr.$$

Here, we keep the counterion density, $\rho_0 e^{-\beta e\psi(r)}$, and the potential, $\psi(r)$, fixed and as obtained by solving the Poisson-Boltzmann equation. We now estimate the inside osmotic pressure by calculating how F varies with ϵ:

$$\left(\frac{\partial F}{\partial \epsilon} \right)_{T,Z} = -\frac{Z k_B T}{z(\epsilon)}\frac{\partial z(\epsilon)}{\partial \epsilon} + 2\pi \epsilon^2 \psi(\epsilon)\, e\rho_0\, e^{-\beta e\psi(\epsilon)}$$

$$\Pi_i = \frac{1}{4\pi \epsilon^2}\left(\frac{\partial F}{\partial \epsilon} \right)_{T,Z}$$

$$= k_B T \rho(\epsilon) - \frac{e}{2}\psi(\epsilon)\rho(\epsilon)$$

$$\overset{\epsilon \to 0}{\to} k_B T\rho(0) - \frac{e}{2}\psi(0)\rho(0). \qquad (9)$$

This result differs from Eq. 7; it has an additional contribution related to the product $\psi(0)\rho(0)$. As a result, Π_i now varies with volume fraction, as shown by the * symbols in Fig. 7. The result remains qualitatively the same to when we only considered the role of the counterions: The difference in osmotic pressure between the outside and inside of the particle remains negative for low particle concentrations, favoring particle swelling, and positive for high particle concentrations, favoring deswelling. In addition, the values obtained at low ϕ are comparable to those obtained experimentally. However, more rigorous calculations of Π_i, which do not rely on our proposal of deflating an inside sphere, would be desirable to confirm the validity of our simple calculations.

VIII. EFFECT OF SALT

The importance of the counterions in our model for deswelling suggests that the addition of salt could have a strong influence. Since the microgel structure is open for ions, salt ions are expected to explore the outside and inside of the microgel. Therefore, the presence of salt at a concentration similar or larger than the average counterion concentration is expected to decrease the osmotic pressure difference between the inside and the outside of the particles [36, 37].

The Poisson-Boltzmann equation including monovalent salt ions can be solved with a procedure analogous to that outlined in section IV. The right-hand side of Eq. 2 changes due to the presence of salt ions:

$$\Delta\psi(\boldsymbol{r}) = -\frac{e}{\epsilon_r \epsilon_0}\left[\rho_+(r) - \rho_-(r) - \rho_f(r) \right] \qquad (10)$$

$$= -\frac{e}{\epsilon_r \epsilon_0}\left[\rho_+ e^{-\beta e\psi(\boldsymbol{r})} - \rho_- e^{\beta e\psi(\boldsymbol{r})} - \rho_f(\boldsymbol{r}) \right],$$

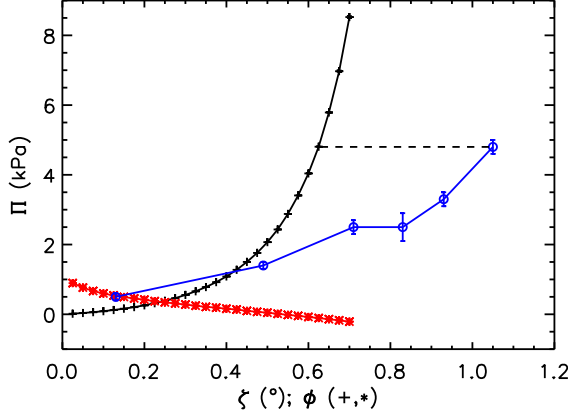where $\rho_+(r)$ and $\rho_-(r)$ are the densities of ions with charge e and $-e$, respectively, and the constants

FIG. 7. (◦) Osmotic pressure obtained from osmometry measurements versus effective volume fraction, ζ, and (+) osmotic pressure obtained from numerical Poisson–Boltzmann calculations as a function of volume fraction, ϕ. The calculated pressure inside the microgels is obtained using Eq. 9 and is shown with (∗) symbols. The dashed horizontal line at the osmotic pressure $\Pi = 4.8$ kPa connects the measurement at $\zeta = 1.05$ and the calculation at $\phi = 0.63$.

ρ_+ and ρ_- are the corresponding densities at $r = R_{\mathrm{c}}$. The iterative solution of the Poisson-Boltzmann equation also applies for the case with salt. However, both ρ_+ and ρ_- need to be adjusted to find the solution, and the condition for charge neutrality changes to $4\pi \int_0^{R_{\mathrm{c}}} dr\, r^2\, \rho_+ \exp\left[-\beta e \psi(r)\right] = Z + S$ and $4\pi \int_0^{R_{\mathrm{c}}} dr\, r^2\, \rho_- \exp\left[\beta e \psi(r)\right] = S$, where S is the number of salt ion pairs per microgel particle.

Poisson-Boltzmann calculations with salt confirm the leveling effect of the salt, as can be seen in Fig. 8a, where ψ inside the particle progressively approaches the value $\psi(R_{\mathrm{c}}) = 0$ as S increases. This is also reflected by the total ion density, $\rho_+(r) + \rho_-(r)$, shown in Fig. 8b, where the rather low salt concentration corresponding to $S = 10^3$ is found to reduce the osmotic pressure difference between the outside and inside of the particle by $\approx 35\%$ according to our simple model for the inside osmotic pressure, Eq. 7. Further, we find a salt concentration ≈ 1 mM corresponding to $S = 10^4$ is sufficient to essentially eliminate the osmotic pressure difference for the Z value used in our calculations, corresponding to $3Z/(4\pi R_{\mathrm{c}}^3 N_{\mathrm{A}}) \approx 6.3$ mM. Therefore, sufficient added salt could suppress the particle deswelling triggered by the overlap of counterion clouds. In this case, the microgels are expected not to deswell until they come into direct contact. Consequently, their direct interaction is expected to determine their deswelling behavior at high concentrations.

A size-dependent shrinking in bidisperse microgel suspensions could, however, be observed even at relatively high salt concentration, since the fuzzy corona contains less crosslinker than the core and is, therefore, the softest part of the microgel particle. Furthermore, larger
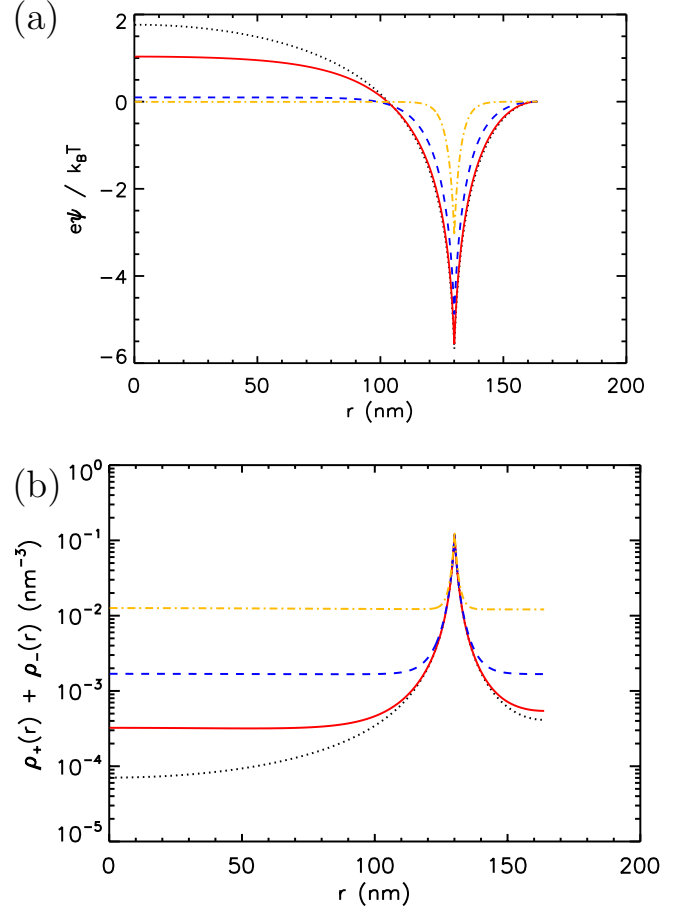

FIG. 8. (a) Electrostatic potential for a microgel with radius 130 nm and fixed charge $-Ze = -70000\,e$ at a volume fraction $\phi = 0.5$ with $S = 10^5$ ($- \cdot -$), $S = 10^4$ ($--$), $S = 10^3$ (—), and without salt ($\cdots$). (b) The corresponding densities of mobile ions, $\rho_+(r) + \rho_-(r)$.

particles are typically softer than smaller ones, if they are synthesized with the same cross-linker concentration: The synthesis of large microgels is continued for longer than for smaller but otherwise identical microgels. This implies that the crosslinker density in the corona of large particles has decayed more than in small particles, further implying that the larger the microgel, the softer the polymer network in its periphery. Whether deswelling is triggered by the osmotic pressure difference between the inside and outside of the particles or due to direct interaction, the largest and softest particles are expected to deswell first and show the most pronounced deswelling. A change in polydispersity is, therefore, expected in either case. Experimental work with charged microgels addressing the swelling behavior with added salt and at high concentrations is thus desirable.

IX. CONCLUSIONS

Counterions originating from charged groups due to ionic initiators employed in the polymerization reaction of pNIPAM are found to cause deswelling of pNIPAM microgels at volume fractions below random close packing. This deswelling also reduces the polydispersity of the suspension, as large particles are usually softer and, therefore, deswell more than smaller ones. Using Poisson-Boltzmann calculations for the counterion clouds and a simple model for the osmotic pressure, we have found that the pressure due to the counterions can explain the observed particle-deswelling at high concentrations. Our calculation of the inside osmotic pressure, however, relies on deflating an inside neutral and impermeable sphere. More rigorous calculations would be desirable to fully assess the validity of our treatment. Within these considerations, our simplified model captures the most important aspects of the spontaneous deswelling process observed experimentally. As completely uncharged pNIPAM microgels are hard to synthesize, our model is expected to apply for most microgels based on pNIPAM without additional charges added to the polymer network. Furthermore, our deswelling mechanism can be expected to also apply to other microgels with an uncharged polymer network but synthesized with an ionic initiator in the absence of significant added salt.

Appendix: A more rigorous calculation of the osmotic pressure inside a charged spherical surface when only considering the contribution of the counterions to the free energy

We consider a spherical cell containing a fixed charge surface-density at $r = R$ representing a charged particle and Z mobile ions. The system is assumed to be charge neutral and all the Coulomb interactions between the ions and between the ions and the charged surface are considered. In addition, the ions are assumed to repel each other like hard spheres. The interaction between the ions i and j carrying z_i and z_j unit charges and having radii R_i and R_j, respectively, is

$$u_{i,j} = \begin{cases} \frac{e^2 z_i z_j}{4\pi\epsilon_0\epsilon_r \, r_{i,j}} & r_{i,j} \geq R_i + R_j \\ \infty & r_{i,j} < R_i + R_j, \end{cases}$$

and the interaction of the ions with the charged surface with radius R is

$$u_{p,i} = \begin{cases} \frac{-e^2 z_i Z}{4\pi\epsilon_0\epsilon_r \, r_i} & r_i \geq R \\ \frac{-e^2 z_i Z}{4\pi\epsilon_0\epsilon_r \, R} & r_i < R. \end{cases}$$

$-Ze$ is the total charge on the surface of the particle, and $e\sum_i z_i = Ze$ due to charge neutrality. With these interactions, we can write the Hamiltonian as: $H = \sum_i u_{p,i} + \sum_{i<j} u_{i,j}$, where we ignore the kinetic energy, as it amounts to a constant average energy. The configurational integral of the N ions is given by

$$\mathcal{Z} = \int_0^{R_c} dr_1 \, r_1^2 ... \int_0^{R_c} dr_N \, r_N^2 \int d\Omega_1 ... \int d\Omega_N e^{-\frac{H}{k_B T}}$$

with the upper integration limit R_c corresponding to the radius of the spherical Wigner-Seitz cell containing the charged particle and the counterions and $d\Omega_i = \sin\theta_i \, d\theta_i \, d\phi_i$ for the integration of the spherical surface areas at $r = r_i$.

To calculate the osmotic pressure in the center of the charged particle, we think of a small, spherical volume with radius ϵ in the center of the particle that is enclosed by a semi-permeable membrane, which is open for the solvent but does not let the ions pass. Therefore, no mobile ions are allowed in this small volume. As a consequence, it has a zero osmotic pressure inside and does not have a Coulomb interaction with any charges, as it is uncharged. However, it has a hard-sphere repulsion with the ions:

$$u_{\epsilon,i} = \begin{cases} \infty & r_i < \epsilon \\ 0 & r_i \geq \epsilon \end{cases}.$$

Due to the infinite repulsion at $r = \epsilon$, the r_i-integrals of the ions now run from ϵ to R_c, and the configurational integral depends on ϵ:

$$\mathcal{Z}(\epsilon) = \int_\epsilon^{R_c} dr_1 \, r_1^2 ... \int_\epsilon^{R_c} dr_N \, r_N^2 \int d\Omega_1 ... \int d\Omega_N e^{-\frac{H}{k_B T}}.$$

Note that the Hamiltonian, H, in the integrand is not affected by the presence of the excluded region at $r < \epsilon$ and that only the integration range changes, since the excluded sphere in the center is uncharged. This differs from the treatment of a similar problem in Ref. [30], where the radius of a *charged* excluded spherical volume is varied and not the radius of an uncharged counterpart.

To calculate the pressure inside the particle, we vary the volume by changing the radius ϵ:

$$\Pi_i = -\left(\frac{\partial F(\epsilon)}{\partial V}\right)_{T,N} = \left(\frac{\partial[k_B T \ln \mathcal{Z}(\epsilon)]}{\partial \epsilon}\right)_{T,N} \frac{d\epsilon}{dV}$$

$$= \frac{-1}{4\pi \, \epsilon^2} \frac{k_B T}{\mathcal{Z}(\epsilon)} \left(\frac{\partial \mathcal{Z}(\epsilon)}{\partial \epsilon}\right)_{T,N},$$

where we have used that $\frac{dV}{d\epsilon} = \frac{4\pi}{3}\frac{d}{d\epsilon}\left(R_c^3 - \epsilon^3\right) = -4\pi \, \epsilon^2$. For the derivative of the configurational integral with respect to ϵ, we assume all counterions to be equivalent with the same valence, $z_i = z$, and we obtain

$$\frac{\partial \mathcal{Z}_\epsilon}{\partial \epsilon} = -\sum_{i=1}^N \int_\epsilon^{R_c} dr_1 \, r_1^2 ... \int_\epsilon^{R_c} dr_N \, r_N^2$$

$$\times \int d\Omega_1 ... \int d\Omega_N \, \delta(r_i - \epsilon)e^{-\frac{H}{k_B T}}$$

$$= -N \int_\epsilon^{R_c} dr_1 \, r_1^2 ... \int_\epsilon^{R_c} dr_N \, r_N^2$$

$$\times \int d\Omega_1 ... \int d\Omega_N \delta(r_1 - \epsilon)e^{-\frac{H}{k_B T}}, \quad \text{(A.1)}$$

where the minus sign appears due to the differentiation with respect to the lower integration limit, and the δ-function fixes the radial distance of one ion at $r_i = \epsilon$. In the last step, we have used that all ions are equivalent and, therefore, give the same contribution.

Due to the radial symmetry of the colloidal particle, the ion density is also radially symmetric. As a consequence, the exact position of the ion fixed on the spherical shell at $r = \epsilon$ does not matter, and the ion density only depends on the radial distance, r, and not on the angles θ and ϕ giving the position of the fixed ion on that spherical shell. For this reason, the result of the integrations is always the same, irrespective of θ_1 and ϕ_1. Therefore, the Ω_1-integral simply contributes a factor 4π, while the r_1-integral gives ϵ^2 due to the δ-function. We obtain

$$
\frac{\partial \mathcal{Z}_\epsilon}{\partial \epsilon} = -4\pi\epsilon^2 \, N \int_\epsilon^{R_c} dr_2 \, r_2^2 ... \int_\epsilon^{R_c} dr_N \, r_N^2 \tag{A.2}
$$
$$
\times \int d\Omega_2 ... \int d\Omega_N \exp\left[-\frac{H(|r_1| = \epsilon, \boldsymbol{r}_2, ..., \boldsymbol{r}_N)}{k_B T}\right].
$$

Now, we use the ion density at position $\boldsymbol{r}$ defined as

$$
\rho(\boldsymbol{r}) = N \int_V d^3 r_1 ... \int_V d^3 r_N \, \delta(\boldsymbol{r}_1 - \boldsymbol{r}) \frac{e^{-\frac{H}{k_B T}}}{\mathcal{Z}(\epsilon)}
$$
$$
= \frac{N}{\mathcal{Z}(\epsilon)} \int_V d^3 r_2 ... \int_V d^3 r_N
$$
$$
\times \exp\left[-\frac{H(\boldsymbol{r}_1 = \boldsymbol{r}, \boldsymbol{r}_2, ..., \boldsymbol{r}_N)}{k_B T}\right].
$$

Here, the $\boldsymbol{r}_1$-integral is absorbed by the δ-function, as the

position of ion 1 is fixed at $\boldsymbol{r}$. In the calculation for $\frac{\partial \mathcal{Z}_\epsilon}{\partial \epsilon}$ in Eq. A.1, the δ-function only absorbs the r_1-integral for the radial distance of ion 1 and not the Ω_1-integral. The integrations for $\rho(\boldsymbol{r})$ are the same as those in Eq. A.2, and we finally obtain

$$
\frac{\partial \mathcal{Z}_\epsilon}{\partial \epsilon} = -4\pi\epsilon^2 \mathcal{Z}(\epsilon)\rho(\epsilon),
$$

which is needed to calculate the pressure

$$
\Pi_i = \frac{-1}{4\pi\,\epsilon^2} \frac{k_B T}{\mathcal{Z}(\epsilon)} \left(\frac{\partial \mathcal{Z}(\epsilon)}{\partial \epsilon}\right)_{T,N}
$$
$$
= k_B T \rho(\epsilon) \overset{\epsilon \to 0}{\Rightarrow} k_B T \rho(0).
$$

In the last step, we take the limit $\epsilon \to 0$, as the excluded volume in the center of the particle has an arbitrarily small radius ϵ.

This more detailed treatment of the osmotic pressure inside the particle agrees with the result obtained with the mean-field approach of the Poisson-Boltzmann theory (Eq. 7), and it shows that Π_i indeed only depends on the ion density in the center of the particle and the temperature when only the contribution due to the counterions is taken into account for the free energy F.

[1] W. G. Hoover, S. G. Gray, and K. W. Johnson, J. Chem. Phys. 55, 1128 (1971).
[2] R. Agrawal and D. A. Kofke, Molecular physics 85, 23 (1995).
[3] L. Fernández, V. Martin-Mayor, and P. Verrocchio, Phys. Rev. Lett. 98, 085702 (2007).
[4] D. M. Heyes and A. C. Branka, Soft Matter 5, 2681 (2009).
[5] H. Senff and W. Richtering, The Journal of Chemical Physics 111, 1705 (1999).
[6] A. Scotti, U. Gasser, E. S. Herman, J. Han, A. Menzel, L. A. Lyon, and A. Fernandez-Nieves, Phys. Rev. E 96, 032609 (2017).
[7] J. C. Pàmies, A. Cacciuto, and D. Frenkel, The Journal of chemical physics 131, 044514 (2009).
[8] M. Urich and A. R. Denton, Soft Matter 12, 9086 (2016).
[9] M. J. Bergman, N. Gnan, M. Obiols-Rabasa, J.-M. Meijer, L. Rovigatti, E. Zaccarelli, and P. Schurtenberger, Nature Communications 9, 5039 (2018).
[10] P. Ziherl and R. D. Kamien, Phys. Rev. Lett. 85, 3528 (2000).
[11] P. Ziherl and R. D. Kamien, J. Phys. Chem. B 105, 10147 (2001).
[12] F. Scheffold, P. Diaz-Leyva, M. Reufer, N. B. Braham,

I. Lynch, and J. L. Harden, Phys. Rev. Lett. 104, 128304 (2010).
[13] A. S. J. Iyer and L. A. Lyon, Angew. Chem. Int. Ed. 48, 4562 (2009).
[14] A. Scotti, U. Gasser, E. S. Herman, M. Pelaez-Fernandez, L. A. Lyon, and A. Fernandez-Nieves, Proc. Natl. Acad. Sci. USA 113, 5576 (2016).
[15] J. Zhou, J. Wei, T. Ngai, L. Wang, D. Zhu, and J. Shen, Macromolecules 45, 6158 (2012).
[16] S. Alexander, P. M. Chaikin, P. Grant, G. J. Morales, P. Pincus, and D. Hone, J. Chem. Phys. 80, 5776 (1984).
[17] R. Pelton, Advances in Colloid and Interface Science 85, 1 (2000).
[18] M. Stieger, W. Richtering, J. Pedersen, and P. Lindner, J. Chem. Phys. 120, 6197 (2004).
[19] J. J. Lietor-Santos, B. Sierra-Martin, R. Vavrin, Z. Hu, U. Gasser, and A. Fernandez-Nieves, Macromolecules 42, 6225 (2009).
[20] J. J. Lietor-Santos, U. Gasser, R. Vavrin, Z. Hu, and A. Fernandez-Nieves, J. Chem. Phys. 133, 034901 (2010).
[21] J. J. Lietor-Santos, B. Sierra-Martin, U. Gasser, and A. Fernandez-Nieves, Soft Matter 7, 6370 (2011).
[22] T. Hoare and R. Pelton, Macromolecules 37, 2544 (2004).
[23] P. S. Mohanty and W. Richtering, J. Phys. Chem. B 112,

14692 (2008).

[24] D. Duracher, A. Elaissari, and C. Pichot, J. Polym. Sci. Part A: Polym. Chem. **37**, 1823 (1999).

[25] E. Siemes, O. Nevskyi, D. Sysoiev, S. K. Turnhoff, A. Oppermann, T. Huhn, W. Richtering, and D. Wöll, Angewandte Chemie International Edition **57**, 12280 (2018).

[26] U. Gasser, J. S. Hyatt, J.-J. Lietor-Santos, E. S. Herman, L. A. Lyon, and A. Fernandez-Nieves, J. Chem. Phys. **141**, 034901 (2014).

[27] M. Andersson and S. L. Maunu, Journal of Polymer Science: Part B: Polymer Physics **44**, 3305 (2006).

[28] A. Scotti, W. Liu, J. S. Hyatt, E. S. Herman, H. S. Choi, J. W. Kim, L. A. Lyon, U. Gasser, and A. Fernandez-Nieves, J. Chem. Phys. **142**, 234905 (2015).

[29] R. A. Marcus, The Journal of Chemical Physics **23**, 1057 (1955).

[30] H. Wennerström, B. Jönsson, and P. Linse, The Journal of Chemical Physics **76**, 4665 (1982).

[31] M. Allen and D. Tildesley, *Computer simulation of liquids* (Oxford University Press, 1987).

[32] A. R. Denton and Q. Tang, J. Chem. Phys. **145**, 164901 (2016).

[33] G. Romeo, L. Imperiali, J.-W. Kim, A. Fernandez-Nieves, and D. A. Weitz, J. Chem. Phys. **136**, 124905 (2012).

[34] T. R. Matzelle, G. Geuskens, and N. Kruse, Macromolecules **36**, 2926 (2003).

[35] B. Sierra-Martin, Y. Laporte, A. B. South, L. A. Lyon, and A. Fernandez-Nieves, Phys. Rev. E **84**, 011406 (2011).

[36] A. R. Denton, Phys. Rev. E. **67**, 011804 (2003).

[37] M. M. Hedrick, J. K. Chung, and A. R. Denton, The Journal of Chemical Physics **142**, 034904 (2015).